INTERNATIONAL JOURNAL FOR NUMERICAL METHODS IN FLUIDS
*Int. J. Numer. Meth. Fluids* **31**: 601–626 (1999)

# MODELLING OF TWO-DIMENSIONAL LAMINAR FLOW USING FINITE ELEMENT METHOD

ROBERT JURJEVIĆ*
*Škurinjskih žrtava 12, HR-51000 Rijeka, Croatia*

## SUMMARY

In this paper, a Galerkin weighted residual finite element numerical solution method, with velocity material time derivative discretisation, is applied to solve for a classical fluid mechanics system of partial differential equations modelling two-dimensional stationary incompressible Newtonian fluid flow. Classical examples of driven cavity laminar flow and laminar flow past a cylinder are presented. Numerical results are compared with data found in the literature. Copyright © 1999 John Wiley & Sons, Ltd.

KEY WORDS: two-dimensional laminar fluid flow; Newtonian incompressible fluid; finite element method; discretisation of velocity material time derivative

## 1. INTRODUCTION

A great part of Earth's interior and its surface is comprised of fluids. An even further look into space shows that stars, interstellar gases, nebulas and galaxies are made mainly of fluids. Many technical devices, technological processes, and generally a great part of human activity, are related to fluids [1].

The theoretical basis of classical fluid mechanics has been defined already at the beginning of the nineteenth century. Even though the fluid was then defined as a continuum, conforming the natural science paradigm of that time, the same theory is in use today describing fluid flow phenomena well enough for present problems in science and technology. According to Feynman's theory of classification [2], the theory of classical fluid mechanics would be rather of phenomenological than of fundamental type. Mathematical principles of classical fluid mechanics can be found in a book by Serin [3].

This paper uses a classical fluid mechanics system of partial differential equations modelling two-dimensional stationary incompressible flow of a Newtonian fluid, which are two two-dimensional stationary incompressible Newtonian fluid flow Navier–Stokes equations and one two-dimensional incompressible continuity equation.

The aim of this paper is to present a numerical solution method for solving partial differential equations modelling the two-dimensional stationary incompressible flow of a Newtonian fluid. Because of the non-linear term in advective acceleration, many schemes were proposed, from local linearization to up-winding techniques [4]. The scheme used in this paper is based on the Galerkin weighted residual method combined with the discretisation of a velocity material time derivative [4–6]. The domain is discretised using two-dimensional

* Correspondence to: Škurinjskih žrtava 12, HR-51000 Rijeka, Croatia.

CCC 0271–2091/99/190601–26$17.50

*Received July 1997*
*Revised September 1997*

quadrilateral parabolic finite elements. Velocity components are approximated on isoparametric and pressure on superparametric finite elements to avoid pressure solution oscillations [5]. Streamlines are determined using a streamfunction [7].

The numerical method is implemented using an ASCII file in–out computer program written in widely portable K&R C computer programming language [8]. Input data preparation and output data presentation have been handled using I-DEAS finite element modelling computer program [9].

## 2. MATHEMATICAL MODEL

### 2.1. Mathematical model consistency

In order to get a feel about the consistency of the classical fluid mechanics theory used in this paper, the following quotation is included:

> 'Our goal is to outline one specific challenge that faces the next generation of applied mathematicians and mathematical physicists. The problem, which we believe is not widely appreciated in these communities is that it is not all certain whether one of the fundamental models of classical mechanics, of wide utility in engineering applications, is actually self-consistent.
>
> The suspect model is embodied in the Navier–Stokes equations of incompressible fluid dynamics. These equations are nothing more than a continuum formulation of Newton's laws of motion for material "trying to get out of its own way". They are a set of non-linear partial differential equations that are thought to describe fluid motion for gases and liquids, from laminar to turbulent flows, on scales ranging from below a millimetre to astronomical lengths. Only for the simplest examples are they soluble, tough, usually corresponding to laminar flows. In many important applications, including turbulence, they must be modified and matched, truncated and closed, or otherwise approximated analytically or numerically in order to extract any predictions. On its own this is not a fundamental barrier, for a good approximation can sometimes be of equal or greater utility than a complicated exact result.
>
> The issue is that is has never been shown that the Navier–Stokes equations in three spatial dimensions, posses smooth solutions starting from arbitrary initial conditions, even very smooth, physically reasonable, initial conditions. It is possible that the equations produce solutions that exhibit finite time singularities. If this occurs, then subsequent evolution may be non-unique, violating the fundamental tenets of Newtonian determinism for this model. Furthermore, finite time singularities in the solutions signal that the equations are generating structures on arbitrarily small scales, contradicting the separation-of-scales assumption used to derive the hydrodynamic equations from microscopic models. It turns out that the non-linear terms that can not be controlled mathematically are precisely those describing what is presumed to be the basic physical mechanism for the generation of turbulence, namely vortex stretching. So what may appear to the applied scientist to be mathematical formalities, i.e. questions of existence and uniqueness and regularity, are actually intimately tied up with the efficacy of the Navier–Stokes equations as a model for fluid turbulence. Whether or not the equations actually do display these pathologies remains an open problem. It has never been proved one way or the other.' [10]

### 2.2. Navier–Stokes equations and continuity equation

A system of partial differential equations modelling the stationary incompressible flow of a Newtonian fluid in a two-dimensional spatial domain $D$, using Descartes rectangular spatial co-ordinates $x$ and $y$, are

$$u\frac{\partial u}{\partial x}+v\frac{\partial u}{\partial y}=-\frac{1}{\rho}\frac{\partial p}{\partial x}+\nu\left(\frac{\partial^2 u}{\partial x^2}+\frac{\partial^2 u}{\partial y^2}\right)+f_x,\quad \forall(x,y)\in D,$$

 

$$\frac{\partial u}{\partial x}+\frac{\partial u}{\partial y}=0, \quad \forall (x, y)\in D, \tag{1}$$
$$u\frac{\partial v}{\partial x}+v\frac{\partial v}{\partial y}=-\frac{1}{\rho}\frac{\partial p}{\partial y}+\nu\left(\frac{\partial^2 v}{\partial x^2}+\frac{\partial^2 v}{\partial y^2}\right)+f_y, \quad \forall (x, y)\in D,$$

where $u$ and $v$ are velocity components, $p$ is pressure, $f_x$ and $f_y$ are body force components, $\rho=$ constant is fluid density and $\nu=$ constant is kinematic viscosity [5]. The first and last equation in (1) are two-dimensional stationary incompressible Newtonian fluid flow Navier–Stokes equations and the second equation in (1) is a two-dimensional incompressible continuity equation.

System (1) is not completely posed until appropriate boundary conditions are specified. Boundary conditions are necessary for both $u$ and $v$ in (1) and they are determined by the physics of the problem [10].

A wide range of two-dimensional stationary incompressible flows of Newtonian fluid can be covered using essential, or Dirichlet's, and natural, or Neumann's, boundary conditions [5].

$$\begin{aligned} &u|S_{\mathrm{d}u}=u_0,\\ &v|S_{\mathrm{d}v}=v_0,\\ &\operatorname{grad} u|S_{nu}\cdot\boldsymbol{n}\equiv\frac{\partial u}{\partial n}=\left(\frac{\partial u}{\partial n}\right)_0,\\ &\operatorname{grad} v|S_{nv}\cdot\boldsymbol{n}\equiv\frac{\partial v}{\partial n}=\left(\frac{\partial v}{\partial n}\right)_0, \end{aligned} \tag{2}$$

where $S=\partial D$ is a two-dimensional spatial domain boundary, $S_{\mathrm{d}u}\subset S$ is a part of boundary $S$ where the function $u$ is known, $S_{\mathrm{d}v}\subset S$ is a part of boundary $S$ where the function $v$ is known, $S_{nu}\subset S$ is a part of boundary $S$ where the function $\partial u/\partial n$ is known, $S_{nv}\subset S$ is a part of boundary $S$ where the function $\partial v/\partial n$ is known [5].

System (1), together with boundary conditions (2), uniquely determines pressure up to an additive constant. Therefore, for unique pressure determination, the following condition has to be used [5]:

$$p(x_0, y_0)=p_0, \tag{3}$$

where $(x_0, y_0)\in D$ is a point in $D$ where $p$ is known.

Knowing parameters $f_x$, $f_y$, $\rho$ and $\nu$, together with boundary conditions (2) and condition (3), the solution $u(x, y)$, $v(x, y)$ and $p(x, y)$ can be obtained in $\bar{D}$.

### 2.3. *Vorticity, enstrophy, streamfunction and streamlines*

A two-dimensional fluid flow vorticity is defined as [7]

$$\omega=\frac{\partial v}{\partial x}-\frac{\partial u}{\partial y}, \quad \forall (x, y)\in D. \tag{4}$$

A global measure of fluid flow vorticity is enstrophy, defined as

$$\int_D \omega^2 \,\mathrm{d}A, \tag{5}$$

where $\omega$ is the two-dimensional fluid flow vorticity.

 

In the absence of moving boundaries, the incompressible Newtonian fluid flow rate of energy dissipation by viscosity is directly proportional to the enstrophy [10], i.e. it is equal to

$$v\rho \int_D \omega^2 \, \mathrm{d}A.$$

The two-dimensional fluid flow streamfunction, $\psi$, is defined as [7]

$$u = \frac{\partial \psi}{\partial y}, \qquad v = -\frac{\partial \psi}{\partial x}, \quad \forall (x, y) \in D. \tag{6}$$

From (4) and (6) it follows that

$$\frac{\partial^2 \psi}{\partial x^2} + \frac{\partial^2 \psi}{\partial y^2} = -\omega, \quad \forall (x, y) \in D. \tag{7}$$

From Poisson partial differential equation (7), knowing velocity components $u$ and $v$ together with appropriate Dirichlet boundary conditions for streamfunction $\psi$, the streamfunction $\psi(x, y)$ can be obtained in $\bar{D}$.

Two-dimensional stationary fluid flow streamlines are defined as sets [5]

$$\{(x, y) \in \bar{D} : \psi(x, y) = \text{constant}\},$$

with the constant parameter defining a single streamline.

### *2.4. Dimensionless parameters*

After defining dimensionless length, time, velocity, pressure and body force variables

$$x^* = \frac{x}{L}, \quad y^* = \frac{y}{L}, \quad t^* = \frac{t}{L/U}, \quad u^* = \frac{u}{U}, \quad v^* = \frac{v}{U}, \quad p^* = \frac{p}{\rho U^2}, \quad f_x^* = \frac{f_x}{U^2/L},$$

$$f_y^* = \frac{f_y}{U^2/L},$$

where $L$ is reference length and $U$ is reference velocity intensity, the partial differential equations in (1) become

$$u^* \frac{\partial u^*}{\partial x^*} + v^* \frac{\partial u^*}{\partial y^*} = -\frac{\partial p^*}{\partial x^*} + \frac{1}{Re}\left(\frac{\partial^2 u^*}{\partial x^{*2}} + \frac{\partial^2 u^*}{\partial y^{*2}}\right) + f_x^*, \quad \forall (x^*, y^*) \in D^*,$$

$$\frac{\partial u^*}{\partial x^*} + \frac{\partial v^*}{\partial y^*} = 0, \quad \forall (x^*, y^*) \in D^*,$$

$$u^* \frac{\partial v^*}{\partial x^*} + v^* \frac{\partial v^*}{\partial y^*} = -\frac{\partial p^*}{\partial y^*} + \frac{1}{Re}\left(\frac{\partial^2 v^*}{\partial x^{*2}} + \frac{\partial^2 v^*}{\partial y^{*2}}\right) + f_y^*, \quad \forall (x^*, y^*) \in D^*,$$

where

$$Re = \frac{UL}{v}$$

is the Reynolds number and $D^*$ is the dimensionless two-dimensional spatial domain [10].

> 'The Reynolds number is a measure of the ratio of the imposed velocity scale $U$ to the "viscous" scale determined by the system size $L$ and the momentum diffusion time $L^2/v$. Alternatively, it may be thought of as a ratio of the driving from the boundary to the damping from the coefficient of viscosity. Low Reynolds numbers mean strong momentum diffusion—alternatively, week driving or

 

strong damping—suggesting dynamically constrained flows. High Reynolds numbers correspond to relatively strongly driven, underdumped systems. Indeed, the singular limit $Re \to \infty$ transforms the Navier–Stokes equations into the conservative Euler equations. Solutions of the Navier–Stokes equations at high Reynolds numbers may appear, locally, similar to inviscid flows solving Euler equations. The boundary conditions for the Navier–Stokes equations are fundamentally different from those for Euler equations, however, and viscous boundary layers are found near rigid walls. This effect of viscosity is a fundamental source of the difference between solutions of the high Reynolds number Navier–Stokes equations and Euler equations.' [10]

## 3. NUMERICAL METHOD

### 3.1. Discretisation of material time derivative

Material time derivative of quantity $f$ in the two-dimensional spatial domain $D$, using Descartes rectangular spatial co-ordinates $x$ and $y$ is defined as

$$\frac{\mathrm{d}f}{\mathrm{d}t} = u\frac{\partial f}{\partial x} + v\frac{\partial f}{\partial y}, \quad \forall (x, y) \in D, \tag{8}$$

where $u$ and $v$ are velocity components.

The material time derivative of quantity $f$ in (8) can be approximated with

$$\frac{\mathrm{d}f(x, y)}{\mathrm{d}t} \simeq \frac{f(x, y) - f(\tilde{x}, \tilde{y})}{\Delta t}, \tag{9}$$

where $\tilde{x} \equiv \varphi(X, Y, t - \Delta t)$ and $\tilde{y} \equiv \chi(X, Y, t - \Delta t)$ are position co-ordinates of a fluid particle—defined for a particle whose position co-ordinates in time instance $t$ are $\tilde{x} \equiv \varphi(X, Y, t)$ and $\tilde{y} \equiv \chi(X, Y, t)$—in time instance $t - \Delta t$ [6], and $\Delta t$ finite 'small' time interval.

Co-ordinates $\tilde{x}$ and $\tilde{y}$ can be approximated with [6]

$$\tilde{x} \simeq x - u(x, y)\Delta t, \qquad \tilde{y} \simeq y - v(x, y)\Delta t. \tag{10}$$

Using (9) to approximate the velocity material time derivative, the partial differential equations (1) can be transformed to

$$\begin{aligned}
&\frac{u - \tilde{u}}{\Delta t} = -\frac{1}{\rho}\frac{\partial p}{\partial x} + \nu\left(\frac{\partial^2 u}{\partial x^2} + \frac{\partial^2 u}{\partial y^2}\right) + f_x, \quad \forall (x, y) \in D, \\
&\frac{\partial u}{\partial x} + \frac{\partial v}{\partial y} = 0, \quad \forall (x, y) \in D, \\
&\frac{v - \tilde{v}}{\Delta t} = -\frac{1}{\rho}\frac{\partial p}{\partial y} + \nu\left(\frac{\partial^2 v}{\partial x^2} + \frac{\partial^2 v}{\partial y^2}\right) + f_y, \quad \forall (x, y) \in D,
\end{aligned} \tag{11}$$

where $\tilde{u} \equiv u(\tilde{x}, \tilde{y})$ and $\tilde{v} \equiv v(\tilde{x}, \tilde{y})$.

### 3.2. The Galerkin weighted residual method

The Galerkin weighted residual method is a numerical technique that can be used to solve a single or a set of partial differential equations. Methods of weighted residuals have been used quite extensively in the field of fluid mechanics [5].

The key idea of the weighted residual method is the approximation of differential equations solution, i.e. unknown functions, with a finite sum of linearly independent functions. Afterwards, the residual functions are defined and their minimum is searched. As a result, a finite set of constants, approximating differential equations solution, can be calculated.

 

To apply the Galerkin weighted residual method to (11) and (1), the two-dimensional spatial domain $\bar{D} = D \cup S$ has to be approximated with a finite number $n_e$ of non-empty closed sets $\bar{D}^e$ so that [5]

$$\bigcup_e \bar{D}^e = \bar{D}' \simeq \bar{D}, \quad e = 1, 2, \ldots, n_e,$$

$$\bar{D}^i \cap \bar{D}^j = S^i \cap S^j, \quad i \neq j,\ 1 \leq i, j \leq n_e,$$

where $S^i$ and $S^j$ are boundaries of $\bar{D}^i$ and $\bar{D}^j$, $S$ is a boundary of $\bar{D}$ and $\bar{D}'$ is an approximation of the set $\bar{D}$. The boundary $S^e$ of set $\bar{D}^e$ is comprised of sides, i.e. of sets whose union is equal to $S^e$ and whose intersection is a point in $S^e$ or an empty set. Neighbourhood sides of set $\bar{D}^e$ are those sides whose intersection is a point in $S^e$.

On $\bar{D}^e$ sides, specific points, called nodes, are chosen. Each side has an equal number of nodes. Nodes are chosen so that intersection of two neighbourhood sides of set $\bar{D}^e$ is the node called the corner node [5]. Sets $\bar{D}^e$ are arranged so that intersection $\bar{D}^i \cap \bar{D}^j = S^i \cap S^j$, $i \neq j$, can be the only common side of sets $\bar{D}^i$ and $\bar{D}^j$, common corner node of sets $\bar{D}^i$ and $\bar{D}^j$, or empty set. Nodes on a non-empty intersection $\bar{D}^i \cap \bar{D}^j = S^i \cap S^j$, $i \neq j$, are common nodes of sets $\bar{D}^i$ and $\bar{D}^j$. The sets $\bar{D}^e$ are called finite elements.

The set of boundary finite elements $b\bar{D}'$ is defined as

$$b\bar{D}' = \{\bar{D}^i \subset \bar{D}' : S^i \cap S' \neq 0\},$$

where $S^i$ is a boundary of $\bar{D}^i$, $S'$ boundary of $\bar{D}'$ and $S^i \cap S' \neq 0$ one or more sides of set $\bar{D}^i$.

Two-dimensional quadrilateral parabolic finite elements are used in this paper.

Two-dimensional quadrilateral parabolic finite element $\bar{D}^e$, using Descartes rectangular spatial co-ordinates $x$ and $y$, is defined as [5]

$$\bar{D}^e = \left\{(x, y) : x = \sum_{i=1}^{8} N_i(\xi, \eta) x_i^e,\ y = \sum_{i=1}^{8} N_i(\xi, \eta) y_i^e\right\}, \tag{12}$$

where $x_i^e$ and $y_i^e$ are node co-ordinates and $N_i(\xi, \eta)$ are shape functions [5],

$$N_i = \begin{cases} (1 + \xi_i \xi)(1 + \eta_i \eta)(\xi_i \xi + \eta_i \eta - 1)/4, & i = 1, 3, 5, 7, \\ (1 + \xi^2)(1 + \eta_i \eta)/2, & i = 2, 6, \\ (1 + \xi_i \xi)(1 + \eta^2)/2, & i = 4, 8, \end{cases} \tag{13}$$

where $\xi_1 = \xi_7 = \xi_8 = \eta_1 = \eta_2 = \eta_3 = -1$, $\xi_2 = \xi_6 = \eta_4 = \eta_8 = 0$, $\xi_3 = \xi_4 = \xi_5 = \eta_5 = \eta_6 = \eta_7 = 1$, and $\xi, \eta \in [-1, 1]$.

Let $f$ be a scalar quantity defined in $\bar{D}^e$.

If $\bar{D}^e$ is defined with (12), in the case of isoparametric finite elements, the quantity $f$ in $\bar{D}^e$ is approximated with

$$f = \sum_{i=1}^{8} N_i(\xi, \eta) f_i^e,$$

where $f_i^e$ are nodal values of $f$ and $N_i(\xi, \eta)$ are shape functions defined in (13).

If $\bar{D}^e$ is defined with (12), in the case of superparametric finite elements, the quantity $f$ in $\bar{D}^e$ is approximated with

$$f = \sum_{i=1}^{4} M_i(\xi, \eta) f_{2(i-1)+1}^e,$$

 

where $f^e_{2(i-1)+1}$ are values of $f$ in corner nodes and $M_i(\xi, \eta)$ are shape functions [5]

$$M_i = (1 + \xi_{2(i-1)+1}\xi)(1 + \eta_{2(i-1)+1}\eta)/4, \quad i = 1, 2, \ldots, 4, \tag{14}$$

where $\xi_1 = \xi_7 = \eta_1 = \eta_3 = = -1$, $\xi_3 = \xi_5 = \eta_5 = \eta_7 = 1$, and $\xi, \eta \in [-1, 1]$.

After having approximated the set $\bar{D}$ with set $\bar{D}'$, boundary conditions (2) and condition (3) are slightly changed.

Boundary conditions (2) become

$$\begin{aligned} &u|S'_{du} = u_0, \\ &v|S'_{dv} = v_0, \\ &\text{grad } u|S'_{nu} \cdot \boldsymbol{n} \equiv \frac{\partial u}{\partial n} = \left(\frac{\partial u}{\partial n}\right)_0, \\ &\text{grad } v|S'_{nv} \cdot \boldsymbol{n} \equiv \frac{\partial v}{\partial n} = \left(\frac{\partial v}{\partial n}\right)_0, \end{aligned} \tag{15}$$

where $S'_{du} \subset S'$ is a part of boundary $S'$ where the value of function $u$ is known, $S'_{dv} \subset S'$ is a part of boundary $S'$ where the value of function $v$ is known, $S'_{nu} \subset S'$ is a part of boundary $S'$ where the value of function $\partial u/\partial n$ is known and $S'_{nv} \subset S'$ is a part of boundary $S'$ where the value of function $\partial v/\partial n$ is known. Functions $u_0$, $v_0$, $(\partial u/\partial n)_0$ and $(\partial v/\partial n)_0$ are defined by their nodal values on boundary $S'$.

Condition (3) becomes

$$p(x_0, y_0) = p_0, \tag{16}$$

where $(x_0, y_0) \in D'$ is node in $D' = \bar{D}' \backslash S'$ where the value of function $p$ is known.

In this paper, functions $u(x, y)$ and $v(x, y)$ in (11) and (1) are approximated using two-dimensional quadrilateral parabolic isoparametric finite elements and function $p(x, y)$ in (11) and (1) is approximated using two-dimensional quadrilateral parabolic superparametric finite elements to avoid pressure solution oscillations [5].

As a result, a set of non-linear algebraic equations is obtained for (11)

$$\boldsymbol{A}\boldsymbol{e} = \boldsymbol{b}, \tag{17}$$

i.e.

$$\mathscr{A}(\boldsymbol{A}^e\boldsymbol{e}^e) = \mathscr{A}(\boldsymbol{b}^e),$$

where

$$\mathscr{A}(\boldsymbol{A}^e\boldsymbol{e}^e) = \boldsymbol{A}e,$$

$$\mathscr{A}(\boldsymbol{b}^e) = \boldsymbol{b},$$

$$\boldsymbol{b}^e = \boldsymbol{f}^e + \boldsymbol{l}^e + \boldsymbol{g}^e + \boldsymbol{h}^e,$$

$$\boldsymbol{A}^e = \begin{bmatrix} \boldsymbol{C}^e_{11} & \boldsymbol{C}^e_{12} & \boldsymbol{0} \\ \boldsymbol{C}^e_{21} & \boldsymbol{0} & \boldsymbol{C}^e_{23} \\ \boldsymbol{0} & \boldsymbol{C}^e_{32} & \boldsymbol{C}^e_{33} \end{bmatrix} + \begin{bmatrix} \boldsymbol{D}^e_{11} & \boldsymbol{0} & \boldsymbol{0} \\ \boldsymbol{0} & \boldsymbol{0} & \boldsymbol{0} \\ \boldsymbol{0} & \boldsymbol{0} & \boldsymbol{D}^e_{33} \end{bmatrix},$$

$$\boldsymbol{C}_{11}^e = \int_{\bar{D}^e} \left( \frac{N_i N_j - N_i \tilde{N}_j}{\Delta t} + (1-\alpha) v \left( \frac{\partial N_i}{\partial x} \frac{\partial N_j}{\partial x} + \frac{\partial N_i}{\partial y} \frac{\partial N_j}{\partial y} \right) \right) \mathrm{d}A, \quad i,j = 1, \ldots, 8,$$

$$\boldsymbol{C}_{12}^e = \int_{\bar{D}^e} (1-\alpha) \frac{N_i}{\rho} \frac{\partial M_i}{\partial x} \, \mathrm{d}A, \quad i = 1, \ldots, 8, \quad j = 1, \ldots, 4,$$

$$\boldsymbol{C}_{21}^e = \int_{\bar{D}^e} M_i \frac{\partial N_j}{\partial x} \, \mathrm{d}A, \quad i = 1, \ldots, 4, \quad j = 1, \ldots, 8,$$

$$\boldsymbol{C}_{23}^e = \int_{\bar{D}^e} M_i \frac{\partial N_j}{\partial y} \, \mathrm{d}A, \quad i = 1, \ldots, 4, \quad j = 1, \ldots, 8,$$

$$\boldsymbol{C}_{32}^e = \int_{\bar{D}^e} (1-\alpha) \frac{N_i}{\rho} \frac{\partial M_j}{\partial y} \, \mathrm{d}A, \quad i = 1, \ldots, 8, \quad j = 1, \ldots, 4,$$

$$\boldsymbol{C}_{33}^e = \boldsymbol{C}_{11}^e,$$

$$\boldsymbol{D}_{11}^e = \int_{S^e \setminus S_{nu}^e} (1-\alpha) \left( - v N_i \frac{\partial N_j}{\partial n} \right) \mathrm{d}s, \quad i,j = 1, \ldots, 8, \quad S^e \setminus S_{nu}^e \in S',$$

$$\boldsymbol{D}_{33}^e = \int_{S^e \setminus S_{nv}^e} (1-\alpha) \left( - v N_i \frac{\partial N_j}{\partial n} \right) \mathrm{d}s, \quad i,j = 1, \ldots, 8, \quad S^e \setminus S_{nv}^e \in S',$$

$$\boldsymbol{l}_1^e = \begin{bmatrix} \boldsymbol{l}_1^e \\ \boldsymbol{0} \\ \boldsymbol{l}_3^e \end{bmatrix},$$

$$\boldsymbol{l}_1^e = \int_{S_{nu}^e} v N_i \left( \frac{\partial u}{\partial n} \right)_0 \mathrm{d}s, \quad i = 1, \ldots, 8, \quad S_{nu}^e \in S',$$

$$\boldsymbol{l}_3^e = \int_{S_{nv}^e} v N_i \left( \frac{\partial v}{\partial n} \right)_0 \mathrm{d}s, \quad i = 1, \ldots, 8, \quad S_{nv}^e \in S',$$

$$\boldsymbol{f}_1^e = \begin{bmatrix} \boldsymbol{f}_1^e \\ \boldsymbol{0} \\ \boldsymbol{f}_3^e \end{bmatrix},$$

$$\boldsymbol{f}_1^e = \int_{\bar{D}^e} N_i f_x \, \mathrm{d}A, \quad i = 1, \ldots, 8,$$

$$\boldsymbol{f}_3^e = \int_{\bar{D}^e} N_i f_y \, \mathrm{d}A, \quad i = 1, \ldots, 8,$$

$$\boldsymbol{h}^e = \begin{bmatrix} \boldsymbol{h}_1^e \\ \boldsymbol{0} \\ \boldsymbol{h}_3^e \end{bmatrix},$$

$$\boldsymbol{h}_1^e = \int_{S^e \setminus S_{nu}^e} \alpha \left( - v N_i \sum_{k=1}^{8} \frac{\partial N_k}{\partial n} u_k^e \right) \mathrm{d}s, \quad i = 1, \ldots, 8, \quad S^e \setminus S_{nu}^e \in S',$$

$$\boldsymbol{h}_3^e = \int_{S^e \setminus S_{nv}^e} \alpha \left( - v N_i \sum_{k=1}^{8} \frac{\partial N_k}{\partial n} v_k^e \right) \mathrm{d}s, \quad i = 1, \ldots, 8, \quad S^e \setminus S_{nv}^e \in S',$$

$$\boldsymbol{g}^e = \begin{bmatrix} \boldsymbol{g}_1^e \\ \boldsymbol{0} \\ \boldsymbol{g}_3^e \end{bmatrix},$$

$$\boldsymbol{g}_1^e = \int_{\bar{D}^e} -\alpha\left(\frac{N_i}{\rho}\sum_{k=1}^{4}\frac{\partial M_k}{\partial x}p^e_{2(k-1)+1} + \nu\left(\frac{\partial N_i}{\partial x}\sum_{k=1}^{8}\frac{\partial N_k}{\partial x}u_k^e + \frac{\partial N_i}{\partial y}\sum_{k=1}^{8}\frac{\partial N_k}{\partial y}u_k^e\right)\right)\mathrm{d}A,$$

$$i = 1, \ldots, 8,$$

$$\boldsymbol{g}_3^e = \int_{\bar{D}^e} -\alpha\left(\frac{N_i}{\rho}\sum_{k=1}^{4}\frac{\partial M_k}{\partial y}p^e_{2(k-1)+1} + \nu\left(\frac{\partial N_i}{\partial x}\sum_{k=1}^{8}\frac{\partial N_k}{\partial x}v_k^e + \frac{\partial N_i}{\partial y}\sum_{k=1}^{8}\frac{\partial N_k}{\partial y}v_k^e\right)\right)\mathrm{d}A,$$

$$i = 1, \ldots, 8,$$

$$\boldsymbol{e}^e = \begin{bmatrix} \boldsymbol{e}_1^e \\ \boldsymbol{e}_2^e \\ \boldsymbol{e}_3^e \end{bmatrix},$$

$$\boldsymbol{e}_1^e = u_i^e, \quad i = 1, \ldots, 8,$$

$$\boldsymbol{e}_2^e = p_i^e, \quad i = 1, \ldots, 4,$$

$$\boldsymbol{e}_3^e = v_i^e, \quad i = 1, \ldots, 8,$$

where

$$\tilde{N}_j(x, y) \simeq N_j(x - u(x, y)\Delta t, y - v(x, y)\Delta t).$$

$\mathscr{A}$ is matrix and vector assembly operator, $\alpha \in [0, 1)$ is a numerical method coefficient proposed by Utnes [6].

Algebraic equation system (17) is non-linear, even if coefficient $\alpha = 0$, since nodal values of functions $u$ and $v$ are used in the calculation of $\tilde{N}_j$.

A similar non-linear algebraic equation system is obtained for (1) [5]

$$\boldsymbol{A}\boldsymbol{e} = \boldsymbol{b}. \tag{18}$$

The difference between non-linear algebraic equation systems (17) and (18) is in matrix $\boldsymbol{C}_{11}^{\mathrm{e}}$, which for the method proposed by Taylor and Hughes [5], is

$$\boldsymbol{C}_{11}^e = \int_{\bar{D}^e}\left(N_i\left(\frac{\partial N_j}{\partial x}\sum_{k=1}^{8}N_k u_k^e + \frac{\partial N_j}{\partial y}\sum_{k=1}^{8}N_k v_k^e\right) + (1-\alpha)\nu\left(\frac{\partial N_i}{\partial x}\frac{\partial N_j}{\partial x} + \frac{\partial N_i}{\partial y}\frac{\partial N_j}{\partial y}\right)\right)\mathrm{d}A,$$

$$i, j = 1, \ldots, 8.$$

To introduce Dirichlet's boundary conditions in (15) and condition (16), non-linear algebraic equation systems (17) and (18) have to be modified as described by Tailor and Hughes [5]. Neumann's boundary conditions in (15) are introduced via $\boldsymbol{l}^{\mathrm{e}}$ vectors.

Solving (17), modified by boundary conditions introduction, one obtains nodal values of functions $u(x, y)$, $p(x, y)$ and $v(x, y)$ approximating the solution of (11).

Solving (18), modified by boundary conditions introduction, one obtains nodal values of functions $u(x, y)$, $p(x, y)$ and $v(x, y)$ approximating the solution of (1).

### *3.3. Iterative procedure*

The iterative procedure used in this paper consists of two stages: the first stage (I) where Equations (11) are solved, and the second stage (II) where Equations (1) are solved. The

 

numerical scheme used in the first stage is a relatively fast convergent scheme, but not as accurate as the numerical scheme used in the second stage. The numerical scheme used in the second stage does not introduce the velocity material time derivative discretisation error present in the first stage, but since it is a slower convergent scheme, it is desirable that it be used together with the numerical scheme used in the first stage.

Solutions of the non-linear algebraic equation systems (17) and (18) are obtained in an iterative procedure. Nodal values of functions $u$, $p$ and $v$ are assumed to be known in matrix $\boldsymbol{A}$ and vector $\boldsymbol{b}$ so that the systems (17) and (18) can be treated as systems of linear algebraic

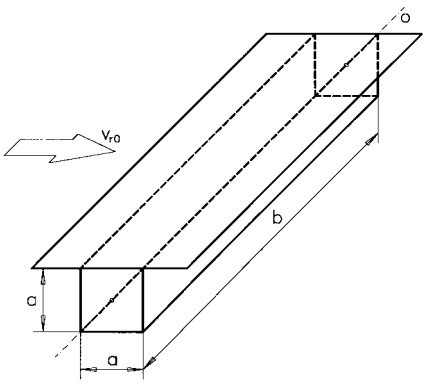


Figure 1. Driven cavity laminar flow.

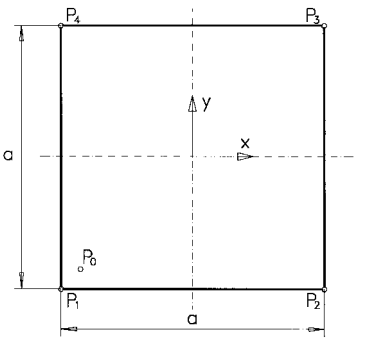


Figure 2. Spatial domain geometry (dclf).

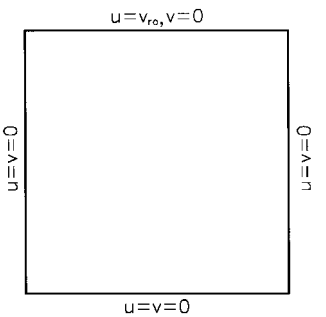


Figure 3. Boundary conditions (dclf).

 

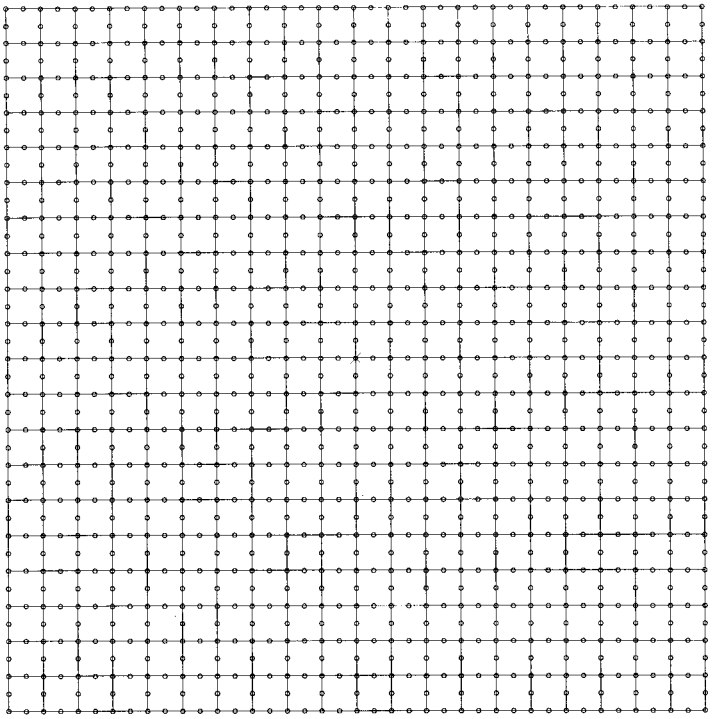

Figure 4. Spatial domain discretisation (dclf).

Table I. Convergence of iterative procedure (dclf-400-1)

| Iteration | $(\Delta u_{ri})_{\max}$ | $(\Delta p_{rj})_{\max}$ | $(\Delta v_{ri})_{\max}$ | Stage |
|---|---|---|---|---|
| 1 | $1.000 \cdot 10^{+4}$ | $1.449 \cdot 10^{+2}$ | $3.414 \cdot 10^{+3}$ | I |
| 2 | $9.583 \cdot 10^{-3}$ | $4.225 \cdot 10^{+0}$ | $9.704 \cdot 10^{-2}$ | I |
| 3 | $5.970 \cdot 10^{-4}$ | $6.080 \cdot 10^{-3}$ | $3.599 \cdot 10^{-5}$ | I |
| 4 | $2.658 \cdot 10^{-7}$ | $4.178 \cdot 10^{-5}$ | $2.345 \cdot 10^{-6}$ | I |
| 1 | $9.696 \cdot 10^{-7}$ | $3.109 \cdot 10^{-5}$ | $2.294 \cdot 10^{-6}$ | II |

equations and as such, solved [11]. The solution of the linear algebraic equation system is then used as new known values of functions $u$, $p$ and $v$ in matrix $\boldsymbol{A}$ and vector $\boldsymbol{b}$ to form a new linear algebraic equation system, which is solved again. The iterative procedure continues until solutions in two consecutive iterations are close enough.

In this paper, the iterative procedure solution is assumed to be reached for given tolerance $\epsilon$ in the $k$th iteration if

$$\Delta u_{ri}^{k} < \epsilon, \quad \forall i = 1, 2, \ldots,$$
$$\Delta p_{rj}^{k} < \epsilon, \quad \forall j = 1, 2, \ldots,$$
$$\Delta v_{ri}^{k} < \epsilon, \quad \forall i = 1, 2, \ldots,$$

where

 

$$\Delta u_{ri}^{k}=\begin{cases}\dfrac{|u_i^{k-1}-u_i^{k}|}{|\boldsymbol{v}_i^{k-1}|} & \text{for} \quad \dfrac{|\boldsymbol{v}_i^{k-1}|}{|\boldsymbol{v}_{r0}|}>\delta \\ \dfrac{|u_i^{k-1}-u_i^{k}|}{\delta|\boldsymbol{v}_{r0}|} & \text{for} \quad \dfrac{|\boldsymbol{v}_i^{k-1}|}{|\boldsymbol{v}_{r0}|}\le\delta\end{cases},$$

$$\Delta p_{rj}^{k}=\begin{cases}\dfrac{|p_j^{k-1}-p_j|}{|p_j^{k-1}|} & \text{for} \quad \dfrac{p_0}{p_1}>0 \quad \text{and} \quad \dfrac{|p_j^{k-1}|}{p_0}>\delta \\ \dfrac{|p_j^{k-1}-p_j^{k}|}{\delta p_0} & \text{for} \quad \dfrac{p_0}{p_1}>0 \quad \text{and} \quad \dfrac{|p_j^{k-1}|}{p_0}\le\delta \\ \dfrac{|p_j^{k-1}-p_j^{k}|}{|p_j^{k-1}|} & \text{for} \quad \dfrac{p_0}{p_1}=0 \quad \text{and} \quad |p_j^{k-1}|>\delta \\ \dfrac{|p_j^{k-1}-p_j^{k}|}{\delta p_1} & \text{for} \quad \dfrac{p_0}{p_1}=0 \quad \text{and} \quad |p_j^{k-1}|\le\delta\end{cases},$$

$$\Delta v_{ri}^{k}=\begin{cases}\dfrac{|v_i^{k-1}-v_i^{k}|}{|\boldsymbol{v}_i^{k-1}|} & \text{for} \quad \dfrac{|\boldsymbol{v}_i^{k-1}|}{|\boldsymbol{v}_{r0}|}>\delta \\ \dfrac{|v_i^{k-1}-v_i^{k}|}{\delta|\boldsymbol{v}_{r0}|} & \text{for} \quad \dfrac{|\boldsymbol{v}_i^{k-1}|}{|\boldsymbol{v}_{r0}|}\le\delta\end{cases},$$

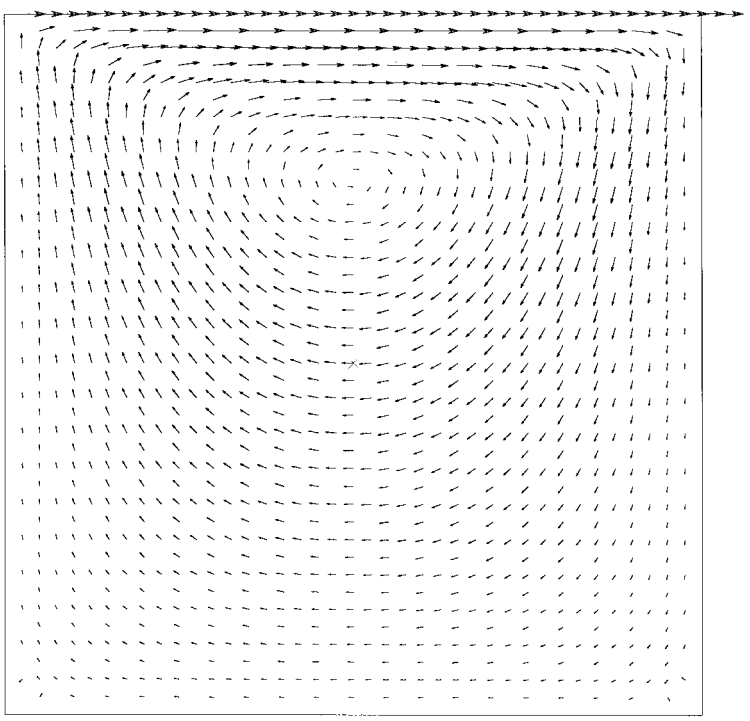

Figure 5. Nodal velocities (dclf-400-1).

 

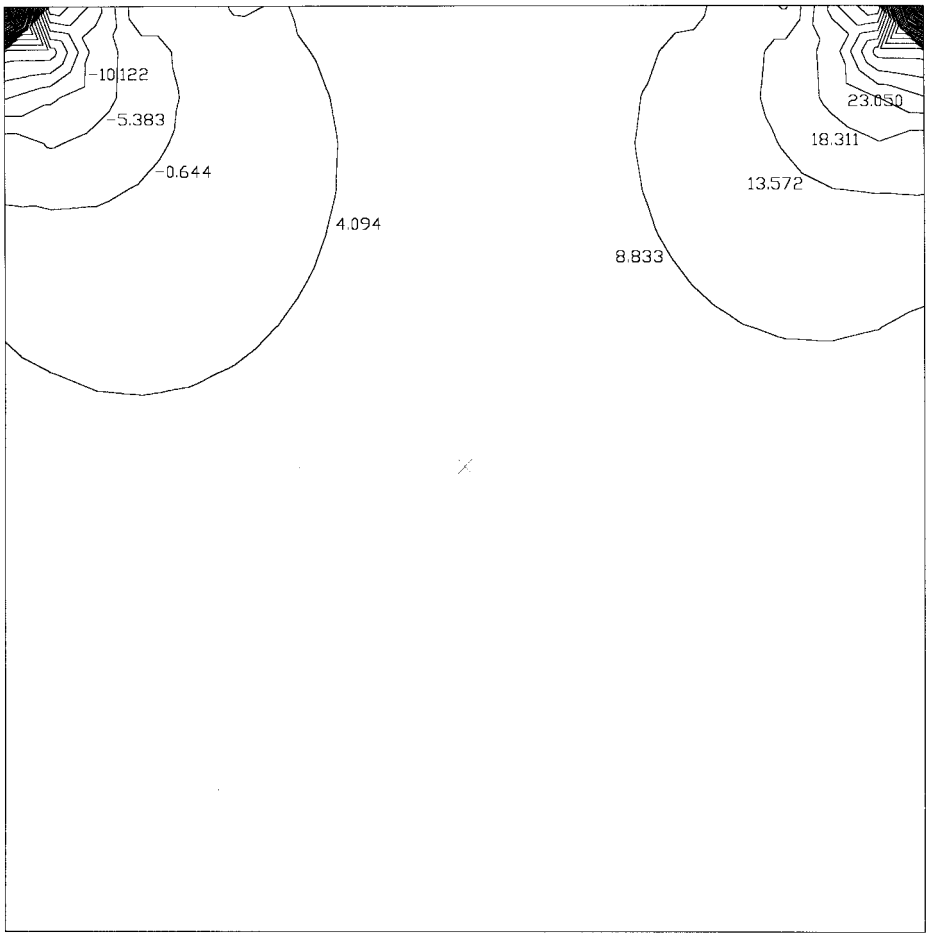


Figure 6. Pressure contours (dclf-400-1).

where $p_0 \geq 0$ Pa is a reference pressure, $p_1 = 1$ Pa is substitution for the reference pressure if $p_0 = 0$ Pa, $\delta = 0.0001$ is the minimal velocity intensity ratio and pressure ratio, $|\boldsymbol{v}_i^{k-1}|$ are velocity intensities at nodes and $|\boldsymbol{v}_{r0}|$ is reference velocity intensity.

The primary sources of error associated with the application of the finite element method are [5]:

- numerical round-off resulting from the necessary numerical manipulations within a computer,
- the tolerance set for the termination of iterative procedure,
- discretisation errors arising from the finite element approximation.

## 4. NUMERICAL EXAMPLES

In this paper a classical example of driven cavity laminar flow and laminar flow past a cylinder are presented.

 

### 4.1. Driven cavity laminar flow (dclf)

A Newtonian incompressible fluid is placed in a rectangular spatial domain, as shown in Figure 1. Three sides are rigid and the fourth one is moving with constant velocity $\boldsymbol{v}_{r0}$. If $b \gg a$, a fluid flow is approximately two-dimensional.

In a two-dimensional model, the spatial domain is a square, shown in Figure 2. Geometry is defined with points: $P_1 \equiv (x_1, y_1)$, $P_2 \equiv (x_2, y_2)$, $P_3 \equiv (x_3, y_3)$ and $P_4 \equiv (x_4, y_4)$, where $x_1 = x_4 = -1$ m, $x_2 = x_3 = 1$ m, $y_1 = y_2 = -1$ m and $y_3 = y_4 = 1$ m. Co-ordinates of point $P_0 \equiv (x_0, y_0)$ are: $x_0 = -0.9$ m and $y_0 = -0.9$ m.

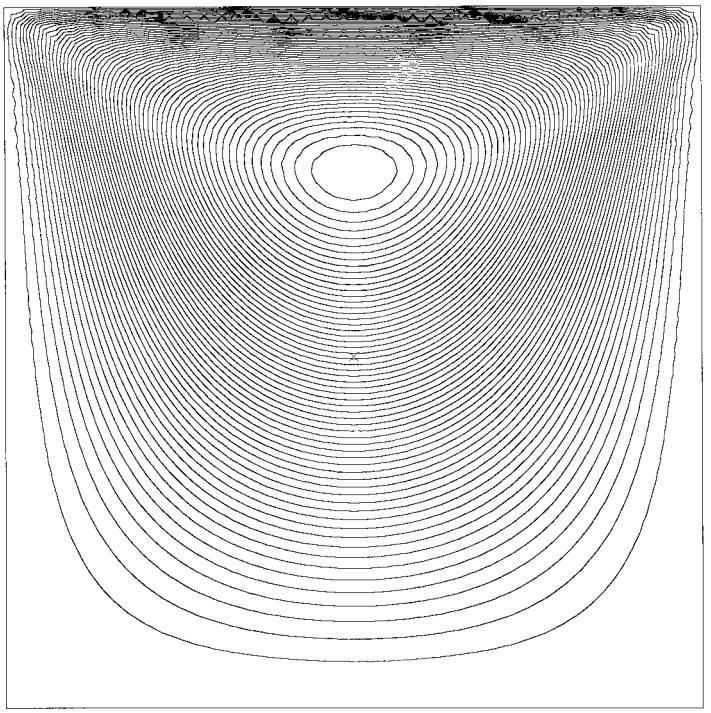

Figure 7. Streamlines (dclf-400-1).

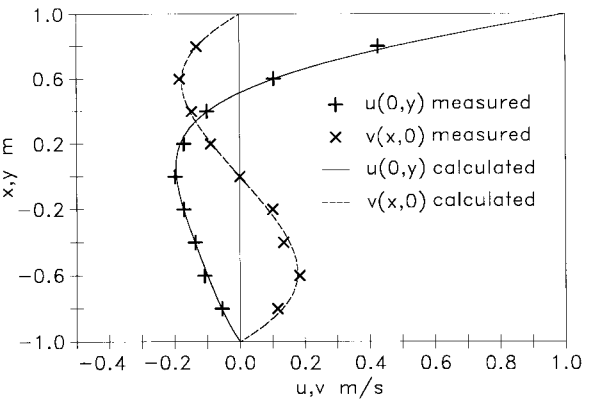


Figure 8. Velocity profiles (dclf-400-1).

 

Table II. Comparison of some calculated data against the literature (dclf-400-1)

| Source | Vertex centre $(x_c, y_c)$ m | $u(0, y)_{\min}$ m s$^{-1}$ | $v(x, 0)_{\min}$ m s$^{-1}$ | $v(x, 0)$ m s$^{-1}$ |
|---|---|---|---|---|
| Author | (0.004, 0.515) | −0.195 | −0.178 | 0.177 |
| [16] | (0.000, 0.500) | −0.199 | −0.177 | 0.177 |
| [17] | (0.000, 0.500) | — | — | — |
| [18] | (0.000, 0.533) | — | — | — |
| [13] | (0.000, 0.540) | −0.188 | −0.175 | 0.175 |

Table III. Convergence of iterative procedure (dclf-400-400)

| Iteration | $(\Delta u_{ri})_{\max}$ | $(\Delta p_{rj})_{\max}$ | $(\Delta v_{ri})_{\max}$ | Stage |
|---|---|---|---|---|
| 1 | $1.000 \cdot 10^{+4}$ | $3.622 \cdot 10^{-1}$ | $3.414 \cdot 10^{+3}$ | I |
| 2 | $1.282 \cdot 10^{+1}$ | $3.589 \cdot 10^{-1}$ | $6.777 \cdot 10^{+0}$ | I |
| 3 | $5.772 \cdot 10^{+0}$ | $1.278 \cdot 10^{-1}$ | $8.758 \cdot 10^{+0}$ | I |
| 4 | $5.301 \cdot 10^{-1}$ | $4.605 \cdot 10^{-2}$ | $5.472 \cdot 10^{-1}$ | I |
| 5 | $2.647 \cdot 10^{-1}$ | $9.472 \cdot 10^{-3}$ | $2.741 \cdot 10^{-1}$ | I |
| 6 | $5.528 \cdot 10^{-2}$ | $2.176 \cdot 10^{-3}$ | $8.168 \cdot 10^{-2}$ | I |
| 7 | $2.027 \cdot 10^{-2}$ | $1.391 \cdot 10^{-3}$ | $2.638 \cdot 10^{-2}$ | I |
| 8 | $4.971 \cdot 10^{-3}$ | $3.474 \cdot 10^{-4}$ | $3.568 \cdot 10^{-3}$ | I |
| 9 | $3.698 \cdot 10^{-3}$ | $9.255 \cdot 10^{-5}$ | $3.086 \cdot 10^{-3}$ | I |
| 10 | $1.809 \cdot 10^{-3}$ | $6.159 \cdot 10^{-5}$ | $1.073 \cdot 10^{-3}$ | I |
| 11 | $7.715 \cdot 10^{-4}$ | $1.812 \cdot 10^{-5}$ | $4.953 \cdot 10^{-4}$ | I |
| 1 | $8.709 \cdot 10^{-4}$ | $2.103 \cdot 10^{-5}$ | $3.770 \cdot 10^{-4}$ | II |

Boundary conditions are shown in Figure 3. The pressure value is prescribed at point $P_0$.

The numerical calculation is performed on discretised spatial domain $\bar{D}'$ comprising of $n_e = 400$ two-dimensional quadrilateral parabolic finite elements, as shown in Figure 4. Functions $u(x, y)$ and $v(x, y)$ are discretised in $n_v = 1281$ nodes and function $p(x, y)$ in $n_p = 441$ nodes.

The Reynolds number for driven cavity two-dimensional flow is

$$Re = \frac{a|\mathbf{v}_{r0}|}{\nu}.$$

*4.1.1. Driven cavity laminar flow (dclf-400-1).* For this particular example, the following data values are chosen: fluid density $\rho = 1$ kg m$^{-3}$, kinematic viscosity $\nu = 2$ m$^2$ s$^{-1}$, body force components $f_x = f_y = 0$ N kg$^{-1}$, tolerance $\epsilon = 0.001$, time interval $\Delta t = 0.00007$ s, numerical scheme coefficient $\alpha = 0$, initial nodal values of functions $u$, $p$ and $v$: $u_i^0 = 0$ m s$^{-1}$, $p_j^0 = 1$ Pa, $v_i^0 = 0$ m s$^{-1}$, $i = 1, 2, \ldots, n_v$, $j = 1, 2, \ldots, n_p$, reference velocity intensity $|\mathbf{v}_{r0}| = 1$ m s$^{-1}$ and reference pressure, defined at point $P_0 \in D'$, $p_0 = 1$ Pa.

Convergence of iterative procedure is shown in Table I.

Calculated fluid flow rate of energy dissipation by viscosity is

$$\nu\rho \int_{D'} \omega^2 \, \mathrm{d}A = 2.5955 \cdot 10^{+1} \text{ W m}^{-1}.$$

The result of the calculation is presented in Figures 5–7. Pressure in Figure 6 is given in Pascals.

A comparison of some calculated data against literature values is given in Figure 8 [12,13] and Table II.

*4.1.2. Driven cavity laminar flow (dclf-400-400).* For this particular example, the following data values are chosen: fluid density $\rho = 1$ kg m$^{-3}$, kinematic viscosity $v = 0.005$ m$^2$ s$^{-1}$, body force components $f_x = f_y = 0$ N kg$^{-1}$, tolerance $\epsilon = 0.001$, time interval $\Delta t = 0.00007$ s, numerical scheme coefficient $\alpha = 0$, initial nodal values of functions $u$, $p$ and $v$: $u_i^0 = 0$ m s$^{-1}$, $p_j^0 = 1$ Pa, $v_i^0 = 0$ m s$^{-1}$, $i = 1, 2, \ldots, n_v$, $j = 1, 2, \ldots, n_p$, reference velocity intensity $|\boldsymbol{v}_{r0}| = 1$ m s$^{-1}$ and reference pressure, defined in point $P_0 \in D'$, $p_0 = 1$ Pa.

Convergence of the iterative procedure is shown in Table III.

Calculated fluid flow rate of energy dissipation by viscosity is

$$v\rho \int_{D'} \omega^2 \, \mathrm{d}A = 8.8787 \cdot 10^{-2} \text{ W m}^{-1}.$$

The result of calculation is presented in Figures 9–11. Pressure in Figure 10 is given in Pascals.

A comparison of some calculated data against literature values is given in Figure 12 [12,13] and Table IV.

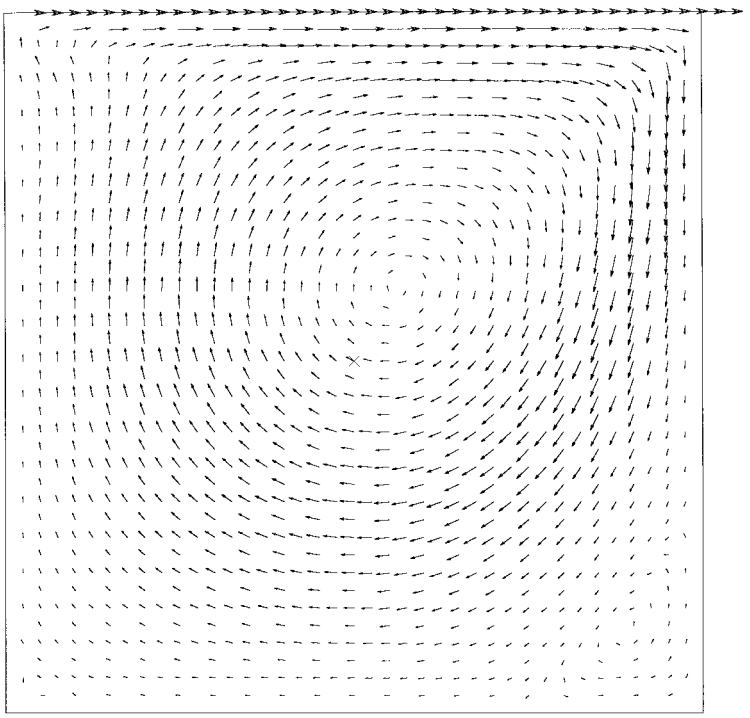

Figure 9. Nodal velocities (dclf-400-400).

 

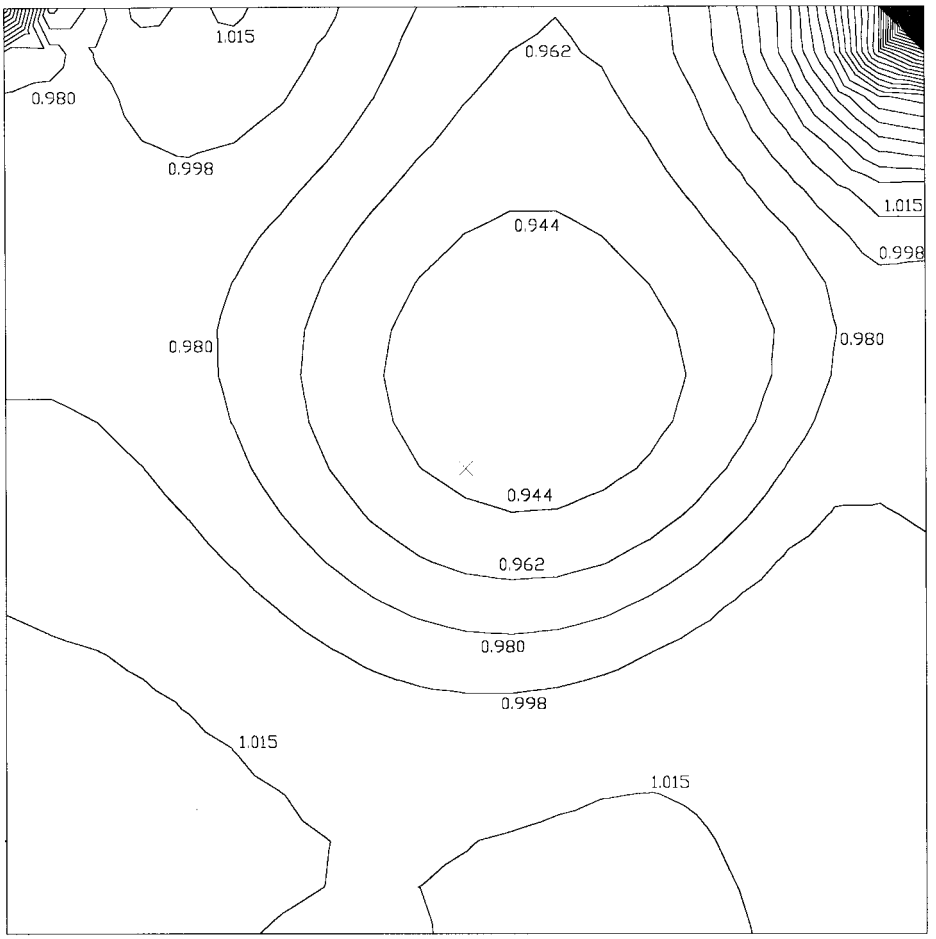


Figure 10. Pressure contours (dclf-400-400).

### *4.2. Laminar flow past a cylinder (lfpc)*

The cylinder of diameter $d$ and breath $b$ is moving in a Newtonian incompressible fluid with constant velocity $\mathbf{v}_{r0}$, as shown in Figure 13.

The co-ordinate system is taken to be fixed on a cylinder. If $b \gg d$ a fluid flow is approximately two-dimensional.

In the two-dimensional model, the spatial domain is a quasi-quadrangle, shown in Figure 14. Since fluid flow is symmetric, just half of the two-dimensional domain is considered [5]. Geometry is defined with points: $P_1 \equiv (x_1, y_1)$, $P_2 \equiv (x_2, y_2)$, $P_3 \equiv (x_3, y_3)$, $P_4 \equiv (x_4, y_4)$, $P_5 \equiv (x_5, y_5)$ and $P_6 \equiv (x_6, y_6)$, where $x_1 = x_6 = -10$ m, $x_2 = -1$ m, $x_3 = 1$ m, $x_4 = x_5 = 20$ m, $y_1 = y_2 = y_3 = y_4 = 0$ m, $y_5 = y_6 = 20$ m. Co-ordinates of point $P_0 \equiv (x_0, y_0)$ are: $x_0 = 16.539$ m, $y_0 = 16.612$ m.

Boundary conditions are shown in Figure 15. The pressure value is prescribed at point $P_0$.

The numerical calculation is performed on discretised spatial domain $\bar{D}'$ comprising of $n_e = 290$ two-dimensional quadrilateral parabolic finite elements, as shown in Figure 16.

 

Functions $u(x, y)$ and $v(x, y)$ are discretised in $n_v = 929$ nodes and function $p(x, y)$ in $n_p = 320$ nodes.

The Reynolds number for two-dimensional laminar flow past a cylinder is

$$Re = \frac{d|\boldsymbol{v}_{r0}|}{\nu}.$$

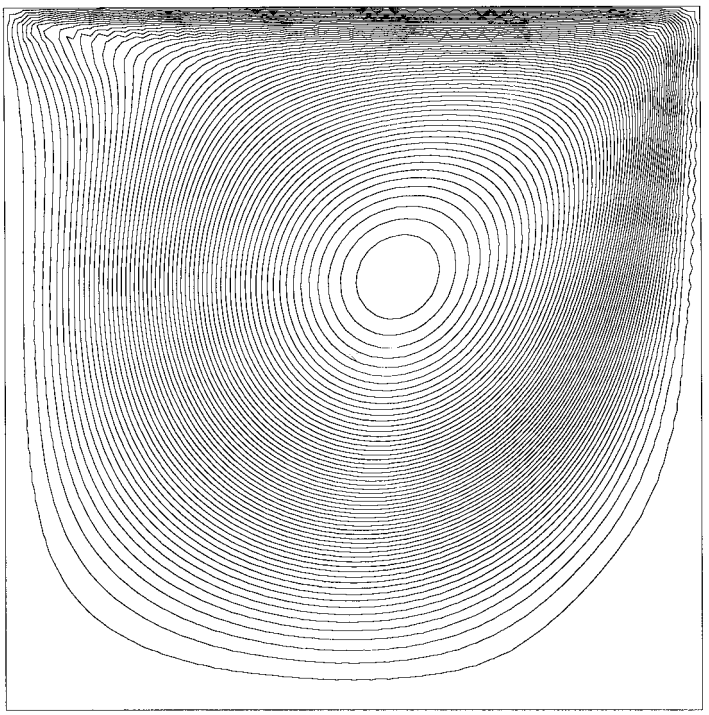

Figure 11. Streamlines (dclf-400-400).

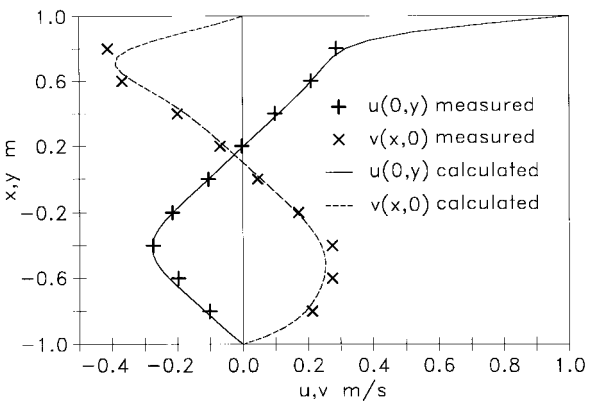


Figure 12. Velocity profiles (dclf-400-400).

 

Table IV. Comparison of some calculated data against the literature (dclf-400-400)

| Source | Vertex centre $(x_c, y_c)$ m | $u(0, y)_{\min}$ m s$^{-1}$ | $v(x, 0)_{\min}$ m s$^{-1}$ | $v(x, 0)_{\max}$ m s$^{-1}$ |
|---|---|---|---|---|
| Author | (0.128, 0.211) | −0.279 | −0.390 | 0.253 |
| [16] | (0.100, 0.200) | −0.285 | −0.390 | 0.250 |
| [12] | (0.120, 0.220) | −0.285 | — | — |
| [19] | (0.109, 0.208) | — | — | — |
| [18] | (0.114, 0.214) | — | — | — |
| [13] | (0.120, 0.240) | −0.300 | −0.450 | 0.293 |

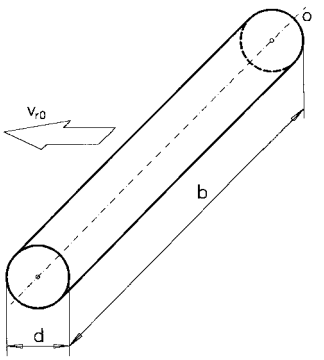


Figure 13. Laminar flow past a cylinder.

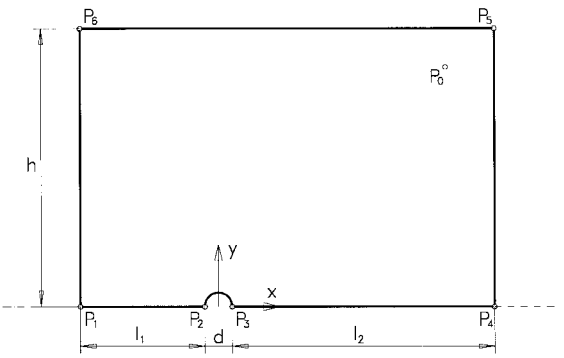


Figure 14. Spatial domain geometry (lfpc).

'At low values of Reynolds number $Re < 0.5$, the inertia forces are negligible and the streamlines converge downstream of the cylinder in a symmetric pattern. If the Reynolds number is in the range $2 < Re < 30$, the boundary layer separates symmetrically and forms two counter-rotating eddies downstream of the cylinder. With increasing Reynolds number, $40 < Re < 70$, the eddies elongate and oscillate laterally. At a certain boundary value $Re \simeq 90$ for a cylinder placed in a free stream, the eddies break from alternate sides of the cylinder and are transported downstream. In a certain range of $Re$ above the limiting value, eddies are continuously shed and form two rows of vortices. The resulting vortex street or vortex trail degenerates at high values of Reynolds number into a random turbulence downstream of the cylinder.' [5]

The following fluid flow types are recognized: stationary, periodic, quasi-periodic and chaotic fluid flow [14,15].

 

*4.2.1. Laminar flow past a cylinder (lfpc-290-1).* For this particular example the following data values are chosen: fluid density $\rho = 1$ kg m$^{-3}$, kinematic viscosity $v = 2$ m$^2$ s$^{-1}$, body force components $f_x = f_y = 0$ N kg$^{-1}$, tolerance $\epsilon = 0.001$, time interval $\Delta t = 0.00011$ s, numerical scheme coefficient $\alpha = 0$, initial nodal values of functions $u$, $p$ and $v$: $u_i^0 = 1$ m s$^{-1}$, $p_j^0 = 1$

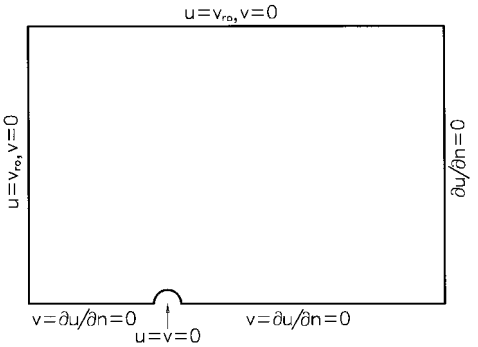


Figure 15. Boundary conditions (lfpc).

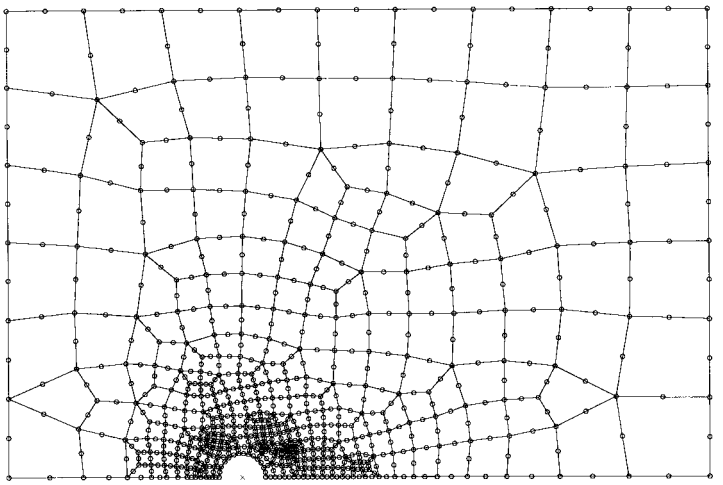

Figure 16. Spatial domain discretisation (lfpc).

Table V. Convergence of iterative procedure (lfpc-290-1)

| Iteration | $(\Delta u_{ri})_{\max}$ | $(\Delta p_{ji})_{\max}$ | $(\Delta v_{ri})_{\max}$ | Stage |
|---|---|---|---|---|
| 1 | $1.000 \cdot 10^{+0}$ | $3.856 \cdot 10^{+0}$ | $3.430 \cdot 10^{-1}$ | I |
| 2 | $3.055 \cdot 10^{-1}$ | $2.580 \cdot 10^{+0}$ | $2.247 \cdot 10^{-1}$ | I |
| 3 | $5.186 \cdot 10^{-3}$ | $1.222 \cdot 10^{-1}$ | $4.293 \cdot 10^{-3}$ | I |
| 4 | $2.656 \cdot 10^{-4}$ | $1.236 \cdot 10^{-2}$ | $1.763 \cdot 10^{-4}$ | I |
| 5 | $1.821 \cdot 10^{-5}$ | $3.632 \cdot 10^{-4}$ | $3.107 \cdot 10^{-5}$ | I |
| 1 | $3.003 \cdot 10^{-3}$ | $8.593 \cdot 10^{-2}$ | $2.064 \cdot 10^{-3}$ | II |
| 2 | $4.180 \cdot 10^{-5}$ | $5.842 \cdot 10^{-3}$ | $1.973 \cdot 10^{-5}$ | II |
| 3 | $2.421 \cdot 10^{-6}$ | $1.646 \cdot 10^{-4}$ | $1.883 \cdot 10^{-6}$ | II |

 

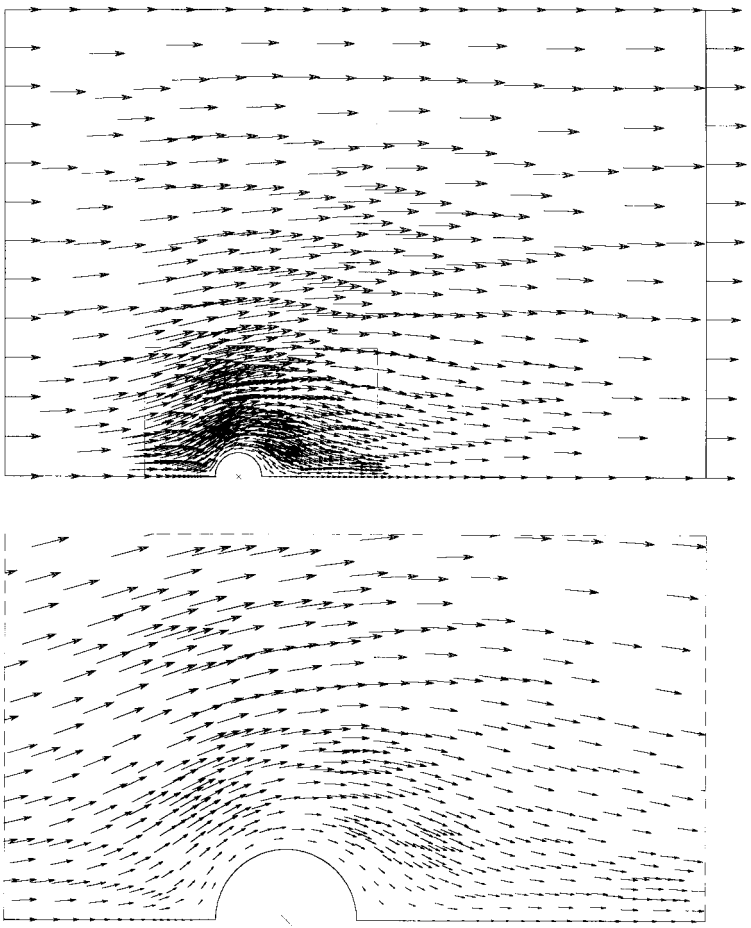

Figure 17. Nodal velocities (lfpc-290-1).

Pa, $v_i^0 = 0$ m s$^{-1}$, $i = 1, 2, \ldots, n_v$, $j = 1, 2, \ldots, n_p$, reference velocity intensity $|\boldsymbol{v}_{r0}| = 1$ m s$^{-1}$ and reference pressure, defined at point $P_0 \in D'$, $p_0 = 1$ Pa.

Convergence of the iterative procedure is shown in Table V.

The calculated fluid flow rate of energy dissipation by viscosity is

$$v\rho \int_{D'} \omega^2 \, \mathrm{d}A = 7.5636 \cdot 10^{+0} \text{ W m}^{-1}.$$

The result of the calculation is presented in Figures 17–19. Pressure in Figure 18 is given in Pascals.

*4.2.2. Laminar flow past a cylinder (lfpc-290-20).* For this particular example, the following data values are chosen: fluid density $\rho = 1$ kg m$^{-3}$, kinematic viscosity $v = 0.1$ m$^2$ s$^{-1}$, body force components $f_x = f_y = 0$ N kg$^{-1}$, tolerance $\epsilon = 0.001$, time interval $\Delta t = 0.00011$ s, numerical scheme coefficient $\alpha = 0$, initial nodal values of functions $u$, $p$ and $v$: $u_i^0 = 1$ m s$^{-1}$, $p_j^0 = 1$ Pa, $v_i^0 = 0$ m s$^{-1}$, $i = 1, 2, \ldots, n_v$, $j = 1, 2, \ldots, n_p$, reference velocity intensity $|\boldsymbol{v}_{r0}| = 1$ m s$^{-1}$ and reference pressure, defined at point $P_0 \in D'$, $p_0 = 1$ Pa.

 

Convergence of the iterative procedure is shown in Table VI.
The calculated fluid flow rate of energy dissipation by viscosity is

$$v\rho \int_{D'} \omega^2 \, \mathrm{d}A = 1.0458 \cdot 10^{+0} \ \mathrm{W\,m^{-1}}.$$

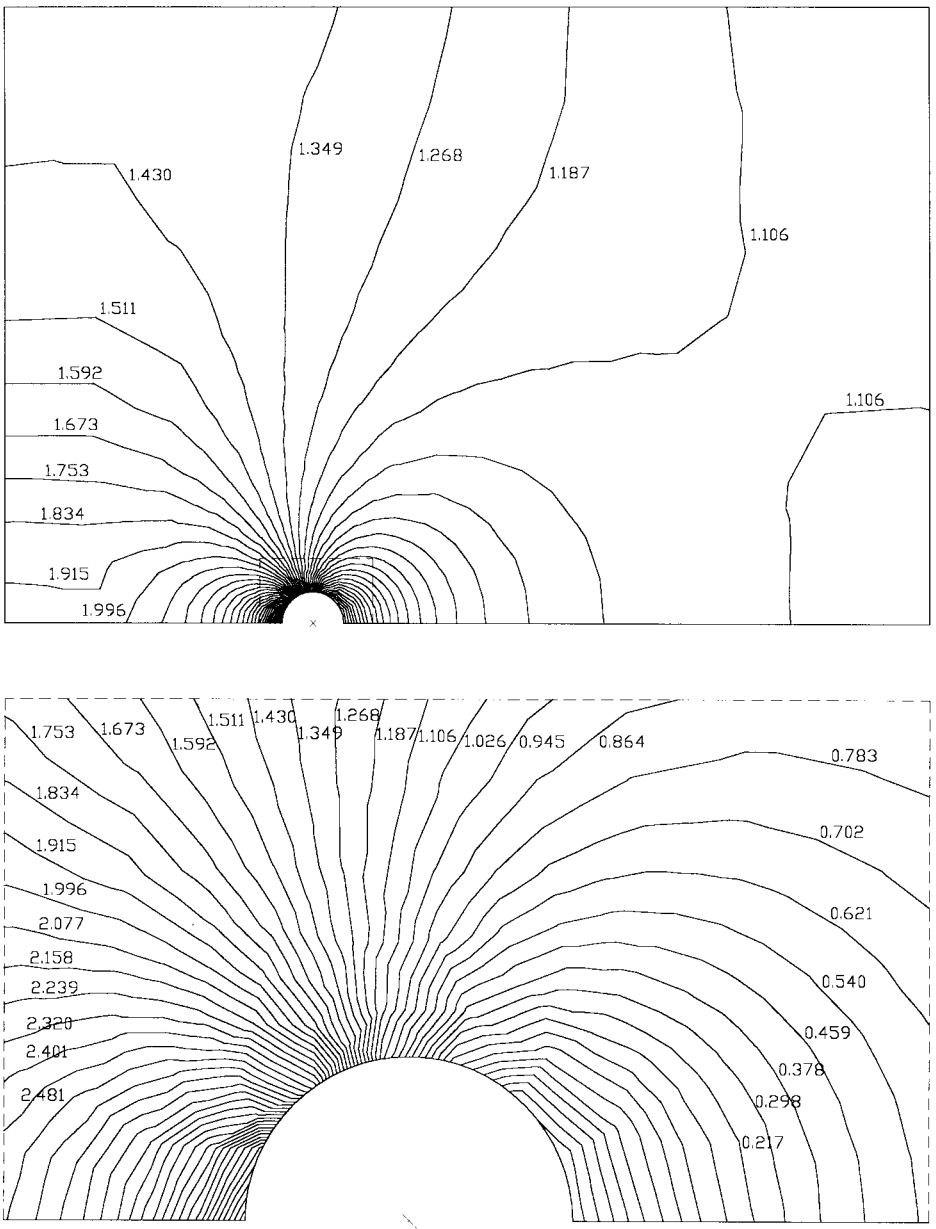


Figure 18. Pressure contours (lfpc-290-1).

 

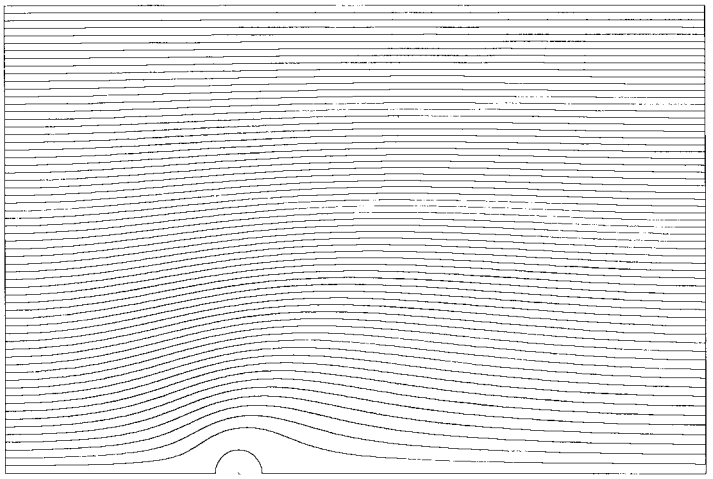

Figure 19. Streamlines (lfpc-290-1).

Table VI. Convergence of iterative procedure (lfpc-290-20)

| Iteration | $(\Delta u_{ri})_{\max}$ | $(\Delta p_{ji})_{\max}$ | $(\Delta v_{ri})_{\max}$ | Stage |
|---|---|---|---|---|
| 1 | $1.016 \cdot 10^{+0}$ | $1.325 \cdot 10^{+0}$ | $5.827 \cdot 10^{-1}$ | I |
| 2 | $2.626 \cdot 10^{+1}$ | $2.335 \cdot 10^{-1}$ | $1.536 \cdot 10^{+0}$ | I |
| 3 | $4.367 \cdot 10^{+0}$ | $1.377 \cdot 10^{-1}$ | $3.526 \cdot 10^{-1}$ | I |
| 4 | $2.747 \cdot 10^{-1}$ | $8.775 \cdot 10^{-3}$ | $5.349 \cdot 10^{-2}$ | I |
| 5 | $4.446 \cdot 10^{-2}$ | $1.684 \cdot 10^{-3}$ | $2.442 \cdot 10^{-2}$ | I |
| 6 | $5.192 \cdot 10^{-2}$ | $6.918 \cdot 10^{-4}$ | $1.322 \cdot 10^{-2}$ | I |
| 7 | $1.350 \cdot 10^{-2}$ | $2.648 \cdot 10^{-4}$ | $2.468 \cdot 10^{-3}$ | I |
| 8 | $3.945 \cdot 10^{-3}$ | $4.146 \cdot 10^{-5}$ | $6.390 \cdot 10^{-4}$ | I |
| 9 | $1.406 \cdot 10^{-4}$ | $1.891 \cdot 10^{-5}$ | $3.219 \cdot 10^{-5}$ | I |
| 1 | $1.802 \cdot 10^{+0}$ | $2.460 \cdot 10^{-2}$ | $3.752 \cdot 10^{-1}$ | II |
| 2 | $5.011 \cdot 10^{-1}$ | $1.481 \cdot 10^{-2}$ | $8.917 \cdot 10^{-2}$ | II |
| 3 | $4.547 \cdot 10^{-1}$ | $5.465 \cdot 10^{-4}$ | $3.233 \cdot 10^{-2}$ | II |
| 4 | $1.312 \cdot 10^{-1}$ | $1.463 \cdot 10^{-4}$ | $3.797 \cdot 10^{-3}$ | II |
| 5 | $3.606 \cdot 10^{-2}$ | $5.155 \cdot 10^{-5}$ | $3.738 \cdot 10^{-4}$ | II |
| 6 | $3.038 \cdot 10^{-3}$ | $1.239 \cdot 10^{-5}$ | $1.886 \cdot 10^{-4}$ | II |
| 7 | $3.394 \cdot 10^{-3}$ | $3.141 \cdot 10^{-6}$ | $9.817 \cdot 10^{-5}$ | II |
| 8 | $9.085 \cdot 10^{-4}$ | $6.381 \cdot 10^{-7}$ | $2.035 \cdot 10^{-5}$ | II |

The result of the calculation is presented in Figures 20–22. Pressure in Figure 21 is given in Pascals.

For this particular example, the numerical calculation is also performed using $n_e = 363$ two-dimensional quadrilateral parabolic finite elements, with $n_v = 1154$ and $n_p = 396$ and using $n_e = 453$ two-dimensional quadrilateral parabolic finite elements, with $n_v = 1444$ and $n_p = 496$.

The calculated fluid flow rates of energy dissipation by viscosity are

$$v\rho \int_{D'} \omega^2 \, \mathrm{d}A = 1.0459 \cdot 10^{+0} \ \mathrm{W\,m^{-1}}.$$

and

 

$$v\rho \int_{D'} \omega^2 \, \mathrm{d}A = 1.0453 \cdot 10^{+0} \ \mathrm{W\,m^{-1}}.$$

respectively.

## 5. CONCLUSIONS

A Galerkin weighted residual finite element numerical solution method for solving classical fluid mechanics partial differential equations modelling two-dimensional stationary incompressible Newtonian fluid flow can be combined with the similar method using discretisation of velocity material time derivative in order to achieve faster convergence and retain acceptable solution accuracy.

A satisfactory fast convergence and numerical solution accuracy has been achieved. As one would expected, a faster convergence and greater numerical solution accuracy is obtained for lower Reynolds numbers. In the case of laminar flow modelling it is observed that the

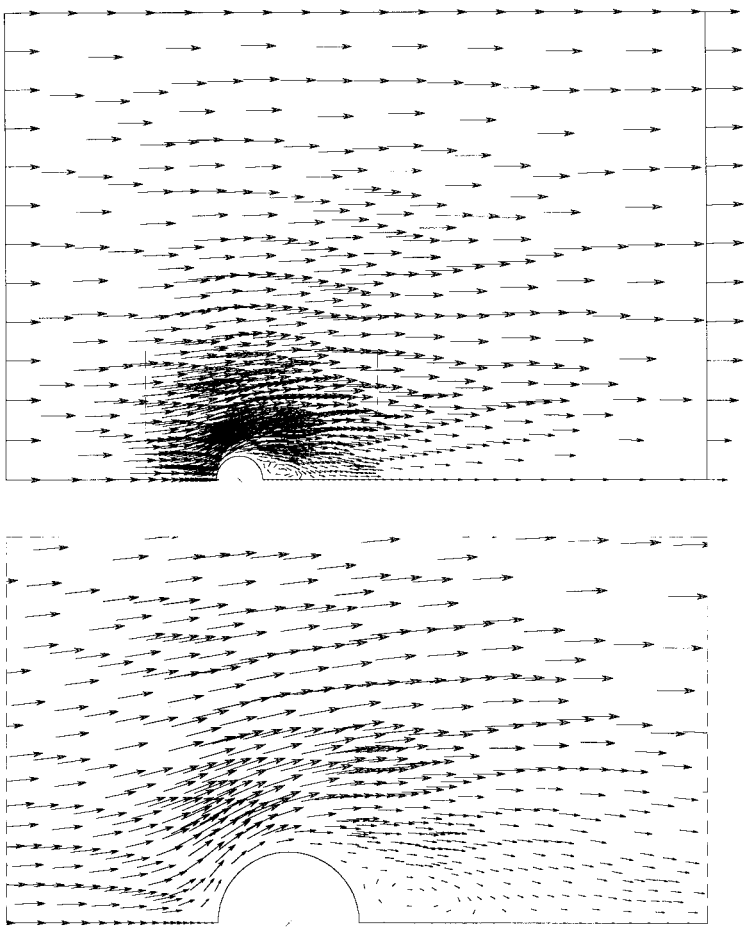

Figure 20. Nodal velocities (lfpc-290-20).

 

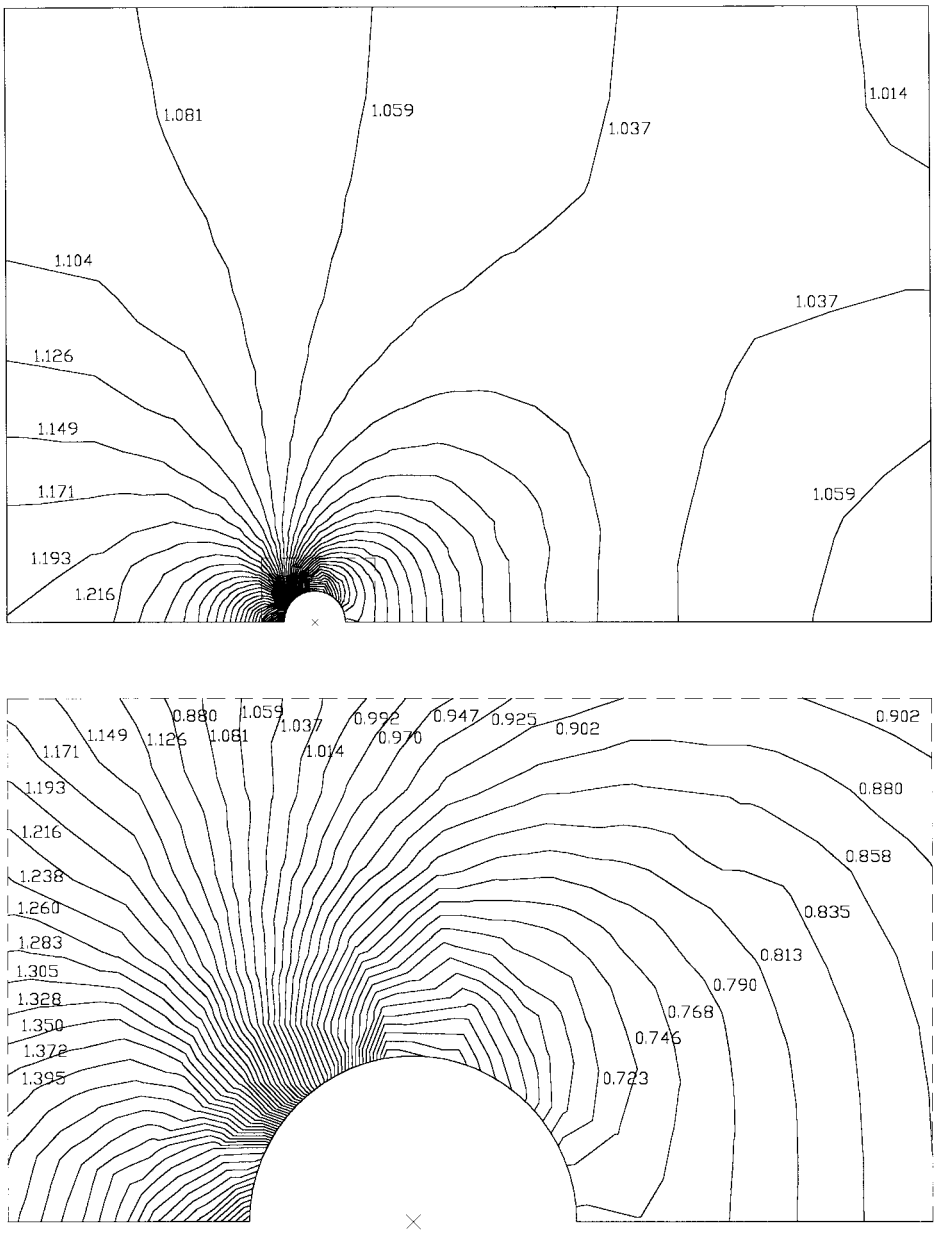


Figure 21. Pressure contours (lfpc-290-20).

numerical method is stable and weakly dependent on velocity material time derivation discretisation time step size.

The implemented numerical method was tested by modelling the driven cavity laminar flow. The numerical results seem to compare favourably with the literature.

 

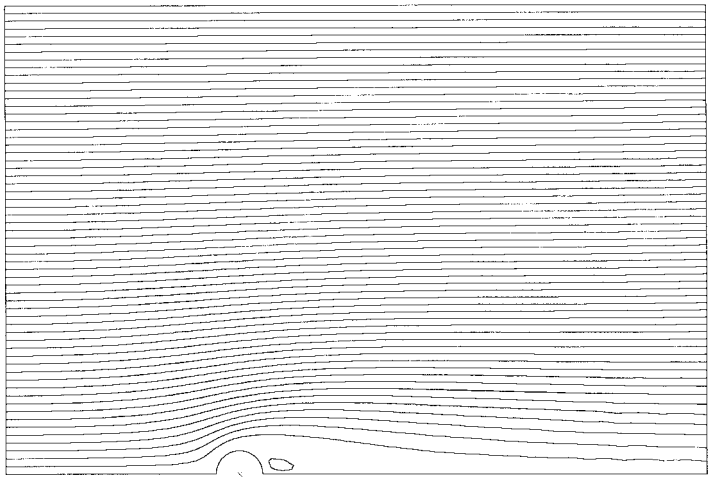

Figure 22. Streamlines (lfpc-290-20).

## REFERENCES


1. W.F. Hughes and J.A. Brighton, *Fluid Dynamics*, McGraw-Hill, New York, 1967.
2. R. Feynman, *The Character of Physical Law*, BBC, London, 1965.
3. J. Serin, *Mathematical Principles of Fluid Mechanics*, Springer, New York, 1959.
4. O. Pironneau, *Finite Element Method for Fluids*, Masson, Paris, 1989.
5. C. Taylor and T.G. Hughes, *Finite Element Programming of the Navier–Stokes Equations*, Pineridge Press, Swansea, 1981.
6. T. Utnes, 'Two-equation ($k$, $\epsilon$) turbulence computations by the use of a finite element model', *Int. J. Numer. Methods Fluids*, **8**, 965–975 (1988).
7. V.L. Streeter and E.B. Wylie, *Fluid Mechanics*, McGraw-Hill, New York, 1985.
8. B.W. Kernighan and D.M. Ritchie, *The C Programming Language*, Prentice-Hall, New Jersey, 1988.
9. Structural Dynamics Research Corporation, *I-DEAS Finite Element Modelling (User's Guide)*, SDRC, Milford, 1990.
10. C.R. Doering and J.D. Gibbon. *Applied Analysis of the Navier–Stokes Equations*, Cambridge University Press, Cambridge, 1995.
11. W.H. Press, B.D. Flamery, S.A. Teukolsky and W.T. Wetterling, *Numerical Recipes*, Cambridge University Press, Cambridge, 1990.
12. O.R. Burggraf, 'Analytical and numerical studies of the structures of steady separated flows', *J. Fluid Mech.*, **24**, 113–151 (1966).
13. S. Sivaloganathan and G.J. Shawl, 'A multigrid method for recirculating flows', *Int. J. Numer. Methods Fluids*, **8**, 417–440 (1988).
14. P. Cvitanović, *Universality in Chaos*, Adam Hilger, Bristol, 1984.
15. W.H. Steeb, *A Handbook of Terms used in Chaos and Quantum Chaos*, BI-Wiss, Mannheim, 1991.
16. D.M. Hawken, H.R. Tamaddon-Jahromi, P. Townsend and M.F. Webster, 'A Taylor–Galerkin-based algorithm for viscous incompressible flow', *Int. J. Numer. Methods Fluids*, **10**, 327–351 (1990).
17. M.M. Gupta and R.P. Manohar, 'Boundary approximations and accuracy in viscous flow computations', *J. Comput. Phys.*, **31**, 265–288 (1979).
18. R. Schreiber and H.B. Keller, 'Driven cavity flows by efficient numerical techniques', *J. Comput. Phys.*, **49**, 310–333 (1983).
19. Hwar-Ching Ku and D. Hatziauramidis, 'Solution of the two-dimensional Navier–Stokes equations by Chebyshev expansion methods', *Comput. Fluids*, **13**, 99–113 (1985).


 